INSTITUTE OF PHYSICS PUBLISHING JOURNAL OF OPTICS A: PURE AND APPLIED OPTICS

J. Opt. A: Pure Appl. Opt. **6** (2004) 475–481 PII: S1464-4258(04)66903-0

The electric and magnetic polarization singularities of paraxial waves

M V Berry

H H Wills Physics Laboratory, University of Bristol, Tyndall Avenue, Bristol BS8 1TL, UK

Received 30 July 2003, accepted for publication 4 September 2003
Published 14 April 2004
Online at stacks.iop.org/JOptA/6/475
DOI: 10.1088/1464-4258/6/5/030

Abstract

For superpositions of electromagnetic plane waves in space whose directions span a small angular range θ, the circular polarization line singularities (of the full and transverse electric and magnetic fields) form clusters, each of four closely-spaced lines. The separations of lines in each cluster are calculated analytically in terms of the transverse electric field and are of the order of $\lambda\theta$—much smaller than the wavelength λ and smaller still than the transverse scale λ/θ of the intensity variations of the field. The electric and magnetic surfaces of transverse linear polarization also lie close together and the separation is calculated analytically, as are the positions on these surfaces of the lines of linear polarization of the full fields. To the two lowest orders in θ, the local wavevector (geometric phase 1-form) is the same for the electric and magnetic fields. The sub-wavelength singular structures are illustrated by numerical calculations.

Keywords: polarization, singularities, electromagnetic, paraxial

1. Introduction

In a seminal paper, Nye and Hajnal [1] discovered that the polarization singularities for typical monochromatic electromagnetic fields in three dimensions are C lines, on which the polarization is purely circular, and L lines, on which the polarization is purely linear. In general the singular lines for the electric field (C_E and L_E, say) and for the magnetic field (C_B and L_B, say) are different. This picture was confirmed in detail by experiments with microwaves [2]. For transverse fields, that is two-dimensional fields, or three-dimensional fields where one component is neglected, the circular polarization lines (now called c_E and c_B) are different from the C_E and C_B lines [3] and the linear polarization singularities are surfaces (ℓ_E and ℓ_B) [4]; these phenomena were also observed [5, 6].

My main purpose here is to explore the interplay of these different situations, as it occurs in paraxial optics (section 2). In this limiting regime, the plane waves into which freely propagating fields can be decomposed span a small range θ of directions, centred on the positive z direction $\mathbf{e}_z$. Then the longitudinal fields E_z, B_z are small in comparison with the transverse fields $\mathbf{E}_t$, $\mathbf{B}_t$. In the approximation of purely transverse fields, in which the z components are neglected, it follows from Maxwell's equations that $\mathbf{E}_t \cdot \mathbf{B}_t = 0$, and this orthogonality implies that the c_E and c_B lines coincide, as do the ℓ_E and ℓ_B surfaces. When the effects of the z components are included to the lowest order in θ, $\mathbf{E}_t$ and $\mathbf{B}_t$ are no longer perpendicular, and the c_E and c_B lines separate and become distinct from the C_E and C_B lines resulting from inclusion of the longitudinal fields (section 3). In addition, the ℓ_E and ℓ_B surfaces separate and, when the longitudinal fields are included, condense onto the L_E and L_B lines (section 4).

In the paraxial approximation, these separation and condensation phenomena can all be described analytically in terms of the transverse electric field $\mathbf{E}_t$ and its transverse derivatives (the alternative choice $\mathbf{B}_t$ would give an equivalent representation).

In section 5, the local wavevector, uniquely defined [1, 7, 8] to be nonsingular at the polarization singularities, is studied in the paraxial approximation. The result is that, although in general the wavevectors are different for the electric and magnetic fields, in the lowest two orders in θ they are the same for the two fields, thereby defining a nontrivial natural position-dependent paraxial propagation direction for the whole electromagnetic field.

Section 6 illustrates the singularity phenomena with numerical calculations.

Let the full electric and magnetic fields in free space, written in terms of the three-dimensional complex fields $\mathbf{E}$

and $\mathbf{B}$, be

$$\begin{gathered}\mathrm{Re}[\mathbf{E}(\mathbf{r},z)\exp\{\mathrm{i}(kz-\omega t)\}],\\ \mathrm{Re}[\mathbf{B}(\mathbf{r},z)\exp\{\mathrm{i}(kz-\omega t)\}],\\ \mathbf{r}=\{x,y\}.\end{gathered}\tag{1}$$

It is convenient to separate the transverse and longitudinal fields, that is

$$\begin{gathered}\mathbf{E}=\{\mathbf{E}_\mathrm{t},E_z\},\qquad \mathbf{B}=\{\mathbf{B}_\mathrm{t},B_z\},\qquad \text{with}\\ \mathbf{E}_\mathrm{t}=\{E_x,E_y\}=\frac{1}{\sqrt{2}}\{E_\mathrm{L}+E_\mathrm{R},-\mathrm{i}(E_\mathrm{L}-E_\mathrm{R})\}\\ \mathbf{B}_\mathrm{t}=\{B_x,B_y\}=\frac{1}{\sqrt{2}}\{B_\mathrm{L}+B_\mathrm{R},-\mathrm{i}(B_\mathrm{L}-B_\mathrm{R})\},\end{gathered}\tag{2}$$

where the left- and right-handed circular components of the fields have been introduced (with the convention that $\{E_x,E_y\}=\{1,\mathrm{i}\}/\sqrt{2}$ is right-handed).

The C and c lines are loci where the full and transverse field vectors are nilpotent, that is [8–10]

$$\begin{gathered}\mathbf{E}\cdot\mathbf{E}=0\quad(\mathrm{C}_E\text{ lines}),\qquad \mathbf{B}\cdot\mathbf{B}=0\quad(\mathrm{C}_B\text{ lines}),\\ \mathbf{E}_\mathrm{t}\cdot\mathbf{E}_\mathrm{t}=2E_\mathrm{L}E_\mathrm{R}=0\quad(\mathrm{c}_E\text{ lines}),\\ \mathbf{B}_\mathrm{t}\cdot\mathbf{B}_\mathrm{t}=2B_\mathrm{L}B_\mathrm{R}=0\quad(\mathrm{c}_B\text{ lines}).\end{gathered}\tag{3}$$

These singularities are lines, because the vanishing of a complex quantity, e.g. $\mathbf{E}\cdot\mathbf{E}$ implies two conditions. The L and ℓ singularities are loci where the real and imaginary parts of the field vectors are parallel, that is

$$\begin{gathered}\mathrm{Im}\,\mathbf{E}^*\times\mathbf{E}=0\quad(\mathrm{L}_E\text{ lines});\\ \mathrm{Im}\,\mathbf{B}^*\times\mathbf{B}=0\quad(\mathrm{L}_B\text{ lines})\\ \mathrm{Im}\,\mathbf{E}_\mathrm{t}^*\times\mathbf{E}_\mathrm{t}=0\quad(\ell_E\text{ surfaces});\\ \mathrm{Im}\,\mathbf{B}_\mathrm{t}^*\times\mathbf{B}_\mathrm{t}=0\quad(\ell_B\text{ surfaces}).\end{gathered}\tag{4}$$

As can easily be seen, the L conditions are equivalent to requiring the parallelism of two real 3-vectors, e.g. $\mathrm{Re}\,\mathbf{E}$ and $\mathrm{Im}\,\mathbf{E}$; this corresponds to two conditions, so the L singularities are lines in space. The ℓ singularities are equivalent to requiring the parallelism of two real 2-vectors, corresponding to one condition, so the ℓ singularities are surfaces in space.

In their original papers, Nye [3, 4] and Nye and Hajnal [1] use slightly different notation for the singularities: C^T and L^T (T for 'true') for what are here called C and L lines, and C lines and S surfaces for what are here called c lines and ℓ surfaces.

2. Paraxial approximation

This has been derived many times; it is summarized here in order to make the representation self-contained and to establish notation. We work with the complex fields defined in (1), with the z direction conveniently chosen, for example as the direction of zero transverse momentum, that is, vanishing integral of the Poynting vector $\mathrm{Re}\,\mathbf{E}^*\times\mathbf{B}$ over the $\mathbf{r}$ plane with z fixed. Paraxiality means that the z variation of the complex fields $\mathbf{E}$ and $\mathbf{B}$ is slow in comparison with the wavelength $\lambda=2\pi/k=2\pi c/\omega$, so the factors involving k in (1) dominate the z derivatives (i.e. formally, k is a large parameter).

Paraxiality enables the longitudinal components of the fields to be approximated in terms of the transverse components, using the Maxwell divergence equation:

$$\begin{gathered}E_z\approx\frac{\mathrm{i}}{k}\nabla_\mathrm{t}\cdot\mathbf{E}_\mathrm{t},\qquad B_z\approx\frac{\mathrm{i}}{k}\nabla_\mathrm{t}\cdot\mathbf{B}_\mathrm{t},\\ \text{where }\nabla_\mathrm{t}=\left\{\frac{\partial}{\partial x},\frac{\partial}{\partial y}\right\}.\end{gathered}\tag{5}$$

Manipulation of the two Maxwell curl equations, incorporating the longitudinal fields (5) (or one of the curl equations, together with the vector paraxial wave equation), now leads to

$$\begin{aligned}\mathbf{B}_\mathrm{t}&=\begin{pmatrix}B_x\\B_y\end{pmatrix}\\ &\approx\frac{1}{c}\begin{pmatrix}-E_y-\frac{1}{2k^2}\left\{\left(\frac{\partial^2}{\partial x^2}-\frac{\partial^2}{\partial y^2}\right)E_y-2\frac{\partial^2}{\partial x\partial y}E_x\right\}\\ E_x-\frac{1}{2k^2}\left\{\left(\frac{\partial^2}{\partial x^2}-\frac{\partial^2}{\partial y^2}\right)E_x+2\frac{\partial^2}{\partial x\partial y}E_y\right\}\end{pmatrix}.\end{aligned}\tag{6}$$

In the lowest paraxial approximation, where the terms in $1/k^2$ are neglected, the transverse fields $\mathbf{E}_\mathrm{t}$ and $\mathbf{B}_\mathrm{t}$ are perpendicular, that is $\mathbf{E}\cdot\mathbf{B}=0$.

A more compact form of (6) can be written in terms of the circular polarization components defined in (2) and complex coordinates

$$\zeta=x+\mathrm{i}y,\qquad \bar{\zeta}=x-\mathrm{i}y.\tag{7}$$

A short calculation gives

$$\begin{aligned}B_\mathrm{L}&\approx\frac{\mathrm{i}}{c}\left(E_\mathrm{L}-\frac{2}{k^2}\frac{\partial^2}{\partial\bar{\zeta}^2}E_\mathrm{R}\right),\\ B_\mathrm{R}&\approx\frac{-\mathrm{i}}{c}\left(E_\mathrm{R}-\frac{2}{k^2}\frac{\partial^2}{\partial\zeta^2}E_\mathrm{L}\right).\end{aligned}\tag{8}$$

Finally, the longitudinal component B_z in (5) can be expressed in terms of the transverse electric field $\mathbf{E}_\mathrm{t}$; to lowest order in k

$$B_z\approx\frac{\mathrm{i}}{kc}\left(\frac{\partial E_x}{\partial y}-\frac{\partial E_y}{\partial x}\right)=-\frac{\mathrm{i}}{kc}\mathbf{e}_z\cdot\nabla_\mathrm{t}\times\mathbf{E}_\mathrm{t}.\tag{9}$$

All components of both fields $\mathbf{E}$ and $\mathbf{B}$ have now been expressed in terms of the transverse electric field $\mathbf{E}_\mathrm{t}$.

3. Circular polarization (c and C) singularities

Consider first the transverse fields. For given z, the c singularities are points in the $\mathbf{r}$ plane. The condition for a c_E point (third equation in (3)) can be written

$$\begin{gathered}E_\mathrm{L}=0\quad(\text{right-handed }\mathrm{c}_E\text{ point}),\\ E_\mathrm{R}=0\quad(\text{left-handed }\mathrm{c}_E\text{ point}).\end{gathered}\tag{10}$$

Similarly, a right-(left-)handed c_B point corresponds to the vanishing of $B_\mathrm{L}(B_\mathrm{R})$. The magnetic transverse components are given by (8). If the contributions in $1/k^2$ are ignored, the conditions for c_E and c_B are the same, so the electric and magnetic c points coincide. With the corrections included, the points separate, in a way now to be calculated.

The c_B points satisfy the fourth equation in (3), namely, to lowest order in k

$$2B_\mathrm{L}B_\mathrm{R}\approx\frac{2}{c^2}\left[E_\mathrm{L}E_\mathrm{R}-\frac{2}{k^2}\left(E_\mathrm{L}\frac{\partial^2}{\partial\zeta^2}E_\mathrm{L}+E_\mathrm{R}\frac{\partial^2}{\partial\bar{\zeta}^2}E_\mathrm{R}\right)\right]=0.\tag{11}$$

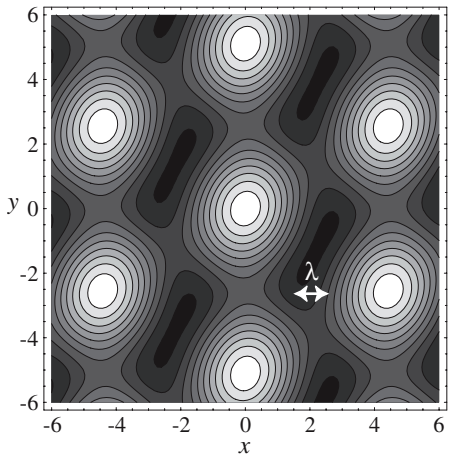

Figure 1. Energy density $\mathbf{E}^* \cdot \mathbf{E} + c^2\mathbf{B}^* \cdot \mathbf{B}$ for the field (36)–(38) with $b_\mathrm{a} = 0.3$, $b_\mathrm{b} = 0.7$, $b_\mathrm{c} = 0.3$ and $\theta = 7.5°$ (x and y in wavelength units).

Consider a right-handed c_E point at $\mathbf{r}_{\mathrm{c}_E}$, that is $E_\mathrm{L}(\mathbf{r}_{\mathrm{c}_E}) = 0$, and let the corresponding c_B point lie at

$$\mathbf{r}_{\mathrm{c}_B} = \mathbf{r}_{\mathrm{c}_E} + \boldsymbol{\delta}_{\mathrm{c}_B}. \tag{12}$$

The shift $\boldsymbol{\delta}_{\mathrm{c}_B}$ can be found by perturbation theory, starting from (11), as the solution of

$$\boldsymbol{\delta}_{\mathrm{c}_B} \cdot \nabla_\mathrm{t} E_\mathrm{L}(\mathbf{r}_{\mathrm{c}_E}) = \frac{2}{k^2}\frac{\partial^2}{\partial\zeta^2} E_\mathrm{R}(\mathbf{r}_{\mathrm{c}_E}). \tag{13}$$

The observation that $\boldsymbol{\delta}_{\mathrm{c}_B}$ is a real vector leads to

$$\boldsymbol{\delta}_{\mathrm{c}_B} = \frac{4\,\mathrm{Im}\big[\mathbf{e}_z \times \nabla_\mathrm{t} E_\mathrm{L}^* \frac{\partial^2}{\partial\zeta^2} E_\mathrm{R}\big]}{k^2\,\mathrm{Im}[\mathbf{e}_z \cdot \nabla_\mathrm{t} E_\mathrm{L}^* \times \nabla_\mathrm{t} E_\mathrm{L}]}, \tag{14}$$

where all quantities are evaluated at $\mathbf{r}_{\mathrm{c}_E}$. For a left-handed c_B point, L and R are interchanged and ζ is replaced by $\bar{\zeta}$.

It is instructive to estimate the magnitude of this splitting of the c_E and c_B points. In a paraxial field whose plane waves span a small angular range θ, the scale of gross features of the field pattern (e.g. the maxima of the field energy density $\mathbf{E}^* \cdot \mathbf{E} + c^2\mathbf{B}^* \cdot \mathbf{B}$) is λ/θ; see figure 1, to be discussed later. Then, using $\partial/\partial x \sim \theta/\lambda$, etc, it follows that the longitudinal field components (5) and (9) are smaller than the transverse components by a factor of the order of θ, and for the $1/k^2$ corrections in (6) the factor is of the order of θ^2, so the paraxial expressions (formally, large k) indeed correspond to small θ. Incorporating this observation into the transverse derivatives in (14) gives

$$\big|\delta_{\mathrm{c}_B}\big| \sim \lambda\theta. \tag{15}$$

This is smaller than the paraxial transverse scale by a factor θ^2 and represents sub-wavelength geometrical structure in the field, as is familiar in singular optics (see, e.g., [11]). All subsequent shifts will have the same order of magnitude.

Consider now the C singularities of the full three-dimensional field, starting with the electric C_E points (again in the **r** plane with given z). From the first equation in (3), and using (5), these satisfy

$$\mathbf{E} \cdot \mathbf{E} = \mathbf{E}_\mathrm{t} \cdot \mathbf{E}_\mathrm{t} + E_z^2 \approx 2E_\mathrm{L}E_\mathrm{R} - \frac{(\nabla_\mathrm{t} \cdot \mathbf{E}_\mathrm{t})^2}{k^2} = 0. \tag{16}$$

Supposing the C_E point to be shifted from the c_E point $\mathbf{r}_{\mathrm{c}_E}$ to

$$\mathbf{r}_{\mathrm{C}_E} = \mathbf{r}_{\mathrm{c}_E} + \boldsymbol{\delta}_{\mathrm{C}_E} \tag{17}$$

(see (12)), perturbation theory gives the shift as

$$\boldsymbol{\delta}_{\mathrm{C}_E} = \frac{\mathrm{Im}[\mathbf{e}_z \times \nabla_\mathrm{t} E_\mathrm{L}^* (\nabla_\mathrm{t} \cdot \mathbf{E}_\mathrm{t})^2]}{k^2\,\mathrm{Im}[\mathbf{e}_z \cdot \nabla_\mathrm{t} E_\mathrm{L}^* \times \nabla_\mathrm{t} E_\mathrm{L}]}. \tag{18}$$

This is for a right-handed C_E point; for a left-handed point, E_L is replaced by E_R.

The magnetic C_B points satisfy the second equation in (3), which with (8) and (9) can be written as

$$\mathbf{B} \cdot \mathbf{B} \approx \frac{2}{c^2}\bigg[E_\mathrm{L}E_\mathrm{R} - \frac{2}{k^2}\bigg(E_\mathrm{L}\frac{\partial^2}{\partial\zeta^2}E_\mathrm{L} + E_\mathrm{R}\frac{\partial^2}{\partial\bar{\zeta}^2}E_\mathrm{R} + \frac{1}{2}(\mathbf{e}_z \cdot \nabla_\mathrm{t} \times \mathbf{E}_\mathrm{t})^2\bigg)\bigg] = 0. \tag{19}$$

Assuming this to be shifted from the electric c_E point to

$$\mathbf{r}_{\mathrm{C}_B} = \mathbf{r}_{\mathrm{c}_E} + \boldsymbol{\delta}_{\mathrm{C}_B}, \tag{20}$$

perturbation theory gives, for a right-handed C_B point,

$$\boldsymbol{\delta}_{\mathrm{C}_B} = \boldsymbol{\delta}_{\mathrm{c}_B} + \frac{\mathrm{Im}[\mathbf{e}_z \times \nabla_\mathrm{t} E_\mathrm{L}^* (\mathbf{e}_z \cdot \nabla_\mathrm{t} \times \mathbf{E}_\mathrm{t})^2]}{k^2\,\mathrm{Im}[\mathbf{e}_z \cdot \nabla_\mathrm{t} E_\mathrm{L}^* \times \nabla_\mathrm{t} E_\mathrm{L}]}; \tag{21}$$

for a left-handed C_B point, E_L is replaced by E_R.

All four of the circular polarization points c_E, c_B, C_E and C_B form a paraxially close cluster, in the sense that all their separations are of the order of $\lambda\theta$ and all points in a cluster have the same handedness.

4. Linear polarization (ℓ and L) singularities

Consider first the transverse fields. For given z, the ℓ singularities are lines in the **r** plane. The condition for a ℓ_E line (third equation in (4)) can be written as

$$\mathrm{Im}\,\mathbf{e}_z \cdot \mathbf{E}_\mathrm{t}^* \times \mathbf{E}_\mathrm{t} = 2\,\mathrm{Im}\,E_x^* E_y = |E_\mathrm{R}|^2 - |E_\mathrm{L}|^2 = 0. \tag{22}$$

The ℓ_B line, slightly displaced from this, satisfies the fourth equation in (4) and can be written

$$|E_\mathrm{R}|^2 - |E_\mathrm{L}|^2 \approx \frac{4}{k^2}\,\mathrm{Re}\bigg(E_\mathrm{R}^*\frac{\partial^2}{\partial\zeta^2}E_\mathrm{L} - E_\mathrm{L}^*\frac{\partial^2}{\partial\bar{\zeta}^2}E_\mathrm{R}\bigg). \tag{23}$$

To calculate the displacement, we again use perturbation theory, starting from a point $\mathbf{r}_{\ell_E}$ on the ℓ_E line. Let δ_{ℓ_B} be the perpendicular displacement of ℓ_B from ℓ_E, in the direction of $\nabla_\mathrm{t}(|E_\mathrm{R}|^2 - |E_\mathrm{L}|^2)$. Then (23) gives

$$\delta_{\ell_B} = \frac{4\,\mathrm{Re}\big(E_\mathrm{R}^*\frac{\partial^2}{\partial\zeta^2}E_\mathrm{L} - E_\mathrm{L}^*\frac{\partial^2}{\partial\bar{\zeta}^2}E_\mathrm{R}\big)}{k^2|\nabla_\mathrm{t}(|E_\mathrm{R}|^2 - |E_\mathrm{L}|^2)|}. \tag{24}$$

For the full three-dimensional fields, the L singularities, for given z, are points in the **r** plane. The L_E points lie on the line ℓ_E (equation (22)) determined by the z component of the first equation in (4); their location on this line is fixed by the x and y components of this vector equation. After using (5), this leads to

$$\mathrm{Re}(\mathbf{E}_\mathrm{t}^* \nabla_\mathrm{t} \cdot \mathbf{E}_\mathrm{t}) = 0. \tag{25}$$

The L_B points lie on the ℓ_B line, which to leading order coincides with the ℓ_E line. The further restriction, locating the points on this line, is the vanishing of the x and y components of the second equality in (4), that is, using (9),

$$\mathrm{Re}(\mathbf{E}_\mathrm{t}^* \mathbf{e}_z \cdot \nabla_\mathrm{t} \times \mathbf{E}_\mathrm{t}) = 0. \tag{26}$$

Because (25) and (26) do not involve k, paraxiality does not imply that the L_E and L_B points lie close to one another.

It might seem that one of the two components of either of the transverse vector equations (25) and (26) is redundant, being implied by the other component, together with the z component (23), since these originate in the first two equations in (4), equivalent to the parallelism of two 3-vectors. But this is not always so; sometimes, the simultaneous vanishing of all three components is required to fix the L_E points, as explained in the appendix to [1].

5. Local wavevectors

With any wave in three dimensions that is not simply plane or spherical, the question arises of specifying a local propagation vector $\mathbf{k}(\mathbf{r}, z)$. Some apparently simple choices [1, 7] are unsatisfactory because they break down on L or C lines. A choice that does not suffer from this defect is an adaptation [7, 12] of the Pancharatnam connection underlying the geometric phase 1-form [13–15]. For the electric field, the wavevector is

$$\begin{aligned}\mathbf{k}_E &= \mathrm{Im}[\mathbf{e}^* \cdot \exp(-\mathrm{i}kz)\nabla(\exp(\mathrm{i}kz)\mathbf{e})] \\ &= k\mathbf{e}_z + \mathrm{Im}[\mathbf{e}^* \cdot \nabla \mathbf{e}],\end{aligned} \tag{27}$$

where the scalar product connects $\mathbf{e}^*$ and $\mathbf{e}$, and

$$\mathbf{e}\,(\mathbf{r}, z) = \frac{\mathbf{E}\,(\mathbf{r}, z)}{\sqrt{\mathbf{E}^*\,(\mathbf{r}, z) \cdot \mathbf{E}\,(\mathbf{r}, z)}} \tag{28}$$

is the locally normalized complex electric field in three dimensions. $\mathbf{k}_E$ is geometric in the sense that it depends only on this locally normalized field, and nonintegrable in the sense that $\nabla \times \mathbf{k}_E \neq 0$. The wavevector $\mathbf{k}_B$ for the magnetic field is defined analogously.

Of principal interest is the transverse component of $\mathbf{k}_E$, namely

$$\mathbf{k}_{E_\mathrm{t}} = \mathrm{Im}\,\mathbf{e}^* \cdot \nabla_\mathrm{t} \mathbf{e}. \tag{29}$$

To approximate this exact expression paraxially, it is convenient to separate the transverse and longitudinal components and introduce the normalized transverse electric field:

$$\mathbf{e}_\mathrm{t} = \frac{\mathbf{E}_\mathrm{t}}{\sqrt{\mathbf{E}_\mathrm{t}^* \cdot \mathbf{E}_\mathrm{t}}}. \tag{30}$$

A short calculation, making use of (5) to eliminate E_z, gives, to order $1/k^2$,

$$\mathbf{k}_{E_\mathrm{t}} \approx \mathrm{Im}[(1 - |\mu|^2)\mathbf{e}_\mathrm{t}^* \cdot \nabla_\mathrm{t} \mathbf{e}_\mathrm{t} + \mu^* \nabla_\mathrm{t} \mu], \tag{31}$$

where

$$\mu = \frac{\nabla \cdot \mathbf{E}_\mathrm{t}}{k\sqrt{\mathbf{E}_\mathrm{t}^* \cdot \mathbf{E}_\mathrm{t}}} = \frac{1}{k}\left(\nabla \cdot \mathbf{e}_\mathrm{t} + \frac{1}{2}\mathbf{e}_\mathrm{t} \cdot \nabla \log \mathbf{E}_\mathrm{t}^* \cdot \mathbf{E}_\mathrm{t}\right). \tag{32}$$

A similar calculation for $\mathbf{k}_B$, using (6) and (9), gives the same result if terms of the order of $1/k^2$ (the terms involving μ) are neglected. Thus

$$\mathbf{k}_E \approx \mathbf{k}_B \approx k\mathbf{e}_z + \mathrm{Im}\,\mathbf{e}_\mathrm{t}^* \cdot \nabla_\mathrm{t} \mathbf{e}_\mathrm{t}. \tag{33}$$

The direction of this vector defines a natural local propagation direction for any paraxial electromagnetic field. Like the exact expression (27), (33) is non-singular everywhere. An attractive feature of (33) is that the transverse component $\mathbf{k}_{E_\mathrm{t}}$ inherits the geometric and nonintegrable features of the full three-dimensional vector $\mathbf{k}_E$.

In terms of the spread θ of the component plane waves, the transverse part $\mathbf{k}_{E_\mathrm{t}}$ is of the order of $k\theta$, so the local direction of $\mathbf{k}_E$ deviates from the z direction by angles of the order of θ, as it should. If terms of the order of $1/k^2$ are included, $\mathbf{k}_E$ and $\mathbf{k}_B$ differ and their directions differ by angles of the order of θ^3. Moreover, the geometric character is lost because of the appearance of the field intensity $\mathbf{E}_\mathrm{t}^* \cdot \mathbf{E}_\mathrm{t}$ in (31) and (32) (and in the corresponding formulae for $\mathbf{k}_{B_\mathrm{t}}$).

6. Numerical illustration

We will explore a slight generalization of a field studied experimentally by Hajnal [2], consisting nominally of three same-handed elliptically polarized plane waves (a, b, c) making the same angle θ with the z axis and symmetrically arrayed around it, that is with wavevectors

$$\begin{aligned}&\mathbf{k}_i = k\{\sin\theta\cos\phi_i, \sin\theta\sin\phi_i, \cos\theta\}, \quad i = \{\mathrm{a}, \mathrm{b}, \mathrm{c}\} \\ &\qquad \phi_\mathrm{a} = \tfrac{1}{6}\pi, \qquad \phi_\mathrm{b} = \tfrac{5}{6}\pi, \qquad \phi_\mathrm{c} = -\tfrac{1}{2}\pi.\end{aligned} \tag{34}$$

The total electric field is

$$\mathbf{E}\,(\mathbf{r}, z) = \mathbf{E}_\mathrm{a} + \mathbf{E}_\mathrm{b} + \mathbf{E}_\mathrm{c}, \tag{35}$$

where

$$\begin{aligned}\mathbf{E}_\mathrm{a} &= \exp\left\{\mathrm{i}k\left(z\cos\theta + \frac{1}{2}x\sin\theta + \frac{\sqrt{3}}{2}y\sin\theta\right)\right\} \\ &\quad \times \{b_\mathrm{a}\mathbf{e}_{1\mathrm{a}} + \mathrm{i}\mathbf{e}_{2\mathrm{a}}\}, \\ \mathbf{E}_\mathrm{b} &= \exp\left\{\mathrm{i}k\left(z\cos\theta - \frac{1}{2}x\sin\theta + \frac{\sqrt{3}}{2}y\sin\theta\right)\right\} \\ &\quad \times \{b_\mathrm{b}\mathbf{e}_{1\mathrm{b}} + \mathrm{i}\mathbf{e}_{2\mathrm{b}}\}, \\ \mathbf{E}_\mathrm{c} &= \exp\{\mathrm{i}k(z\cos\theta - y\sin\theta)\}\{\mathbf{e}_{1\mathrm{c}} + \mathrm{i}b_\mathrm{c}\mathbf{e}_{2\mathrm{c}}\}.\end{aligned} \tag{36}$$

The degree of polarization of the waves is specified by the ellipticities $\sqrt{(1 - b_i^2)}$, with ellipse axes determined by the orthogonal directions (perpendicular to $\mathbf{k}_i$)

$$\begin{aligned}\mathbf{e}_{1i} &= \frac{\mathbf{e}_x\cos\theta - \mathbf{e}_z\sin\theta\cos\phi_i}{\sqrt{\cos^2\theta + \sin^2\theta\cos^2\phi_i}}, \\ \mathbf{e}_{2i} &= \frac{-\mathbf{e}_x\sin^2\theta\sin\phi_i\cos\phi_i + \mathbf{e}_y\left(\cos^2\theta + \sin^2\theta\cos^2\phi_i\right)}{\sqrt{\cos^2\theta + \sin^2\theta\cos^2\phi_i}} \\ &\quad - \frac{\mathbf{e}_z\cos\theta\sin\theta\sin\phi_i}{\sqrt{\cos^2\theta + \sin^2\theta\cos^2\phi_i}}.\end{aligned} \tag{37}$$

For the fields $\mathbf{E}_\mathrm{a}$ and $\mathbf{E}_\mathrm{b}$, the long axes of the polarization ellipses, projected onto the $\mathbf{r}$ plane, are parallel to the x axis;

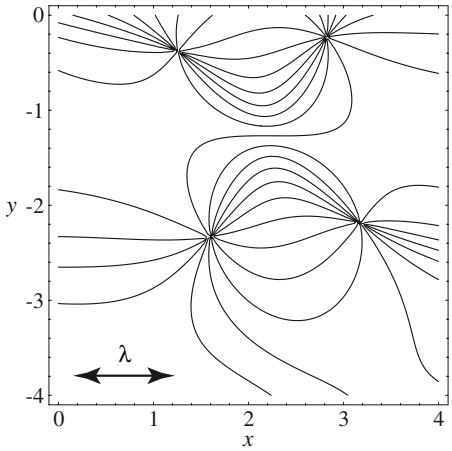

Figure 2. Zero contours of real and imaginary parts of $Q = (\mathbf{E}_t \cdot \mathbf{E}_t)(\mathbf{B}_t \cdot \mathbf{B}_t)(\mathbf{E} \cdot \mathbf{E})(\mathbf{B} \cdot \mathbf{B})$, for the field of figure 1, over a magnified range. Intersections mark the zeros of Q, which are the circular polarization singularities of the field; 16 lines enter the apparent singularities, indicating that each is an unresolved cluster of four elementary singularities.

for $\mathbf{E}_c$, the long axis is parallel to the y axis. In Hajnal's experiment [2], the nominal values of the parameters were $\theta = 15°$, $b_a = b_b = b_c = 0.8$ (i.e. eccentricity 0.6). With the convention in (2) (opposite to Hajnal's), all polarizations are right-handed for $b_i > 0$.

The corresponding magnetic field is $\mathbf{B} = \mathbf{B}_a + \mathbf{B}_b + \mathbf{B}_c$, where

$$\mathbf{B}_i = \frac{\mathbf{k}_i \times \mathbf{E}_i}{ck}. \tag{38}$$

Since for all field components the z dependence consists of the same phase factor, all polarization singularities are independent of z (lines c, C and L, and surfaces ℓ); therefore it suffices to study these in the **r** plane (points c, C and L, and lines ℓ).

In numerical computations, we will work with the exact fields, even for small θ. To evaluate the theoretical expressions for the separations of the singularities, derived in sections 3 and 4, it suffices to use the small-θ limiting form for the transverse electric field, ignoring the irrelevant z dependence, namely

$$\mathbf{E}_{t,\text{paraxial}}(\mathbf{r}) = \exp\left\{ik\theta\left(\frac{1}{2}y + \frac{\sqrt{3}}{2}x\right)\right\}\{b_a, i\} + \exp\left\{ik\theta\left(\frac{1}{2}y - \frac{\sqrt{3}}{2}x\right)\right\}\{b_b, i\} + \exp\{-ik\theta y\}\{i, b_c\}. \tag{39}$$

Figure 1 shows the power distribution in an electromagnetic field of the form (36)–(38), with three different polarization ellipses. The variations are roughly on the expected paraxial scale $\lambda/\theta \sim 7.6$ and there is no hint of the fine-scale singularity phenomena being explored here.

Figure 2 shows a three-fold linear magnification, plotting instead the zeros of the real and imaginary parts of the product Q of all four complex quantities in (3). At each of the separate c and C singularities, the Re Q and Im Q contours cross, so four lines should be attached to each singularity. In figure 2, however, 16 lines appear attached to the singularities, suggesting that each is an unresolved cluster of four.

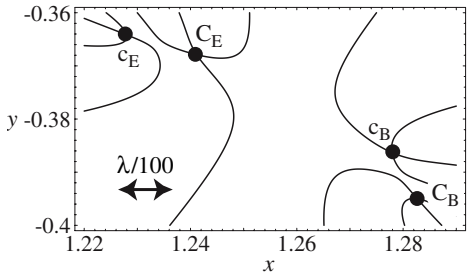

Figure 3. Magnification of the top left cluster of figure 3, revealing the four c and C singularities.

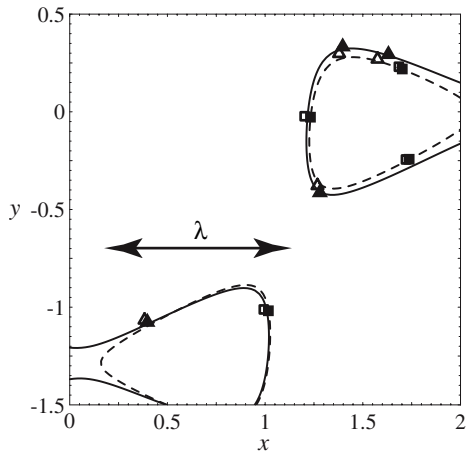

Figure 4. Linear polarization singularities for the field of figure 1 but with $\theta = 15°$, showing ℓ_E lines (full curves), ℓ_B lines (broken curves), L_E points (triangles) and L_B points (squares); full symbols are numerical calculations and open symbols are the theoretical singularities, calculated from the theory of section 4.

Table 1. Displacements of circular polarization singularities in figure 3 from the c_E point, for the fields (29)–(31) with $b_a = 0.3$, $b_b = 0.7$, $b_c = 0.3$ and $\theta = 7.5°$, compared with the theory given in section 3.

	Numerical	Theory	Numerical/ theory
δ_{c_B}	{0.0499, −0.0222}	{0.0500, −0.0221}	{0.998, 1.002}
δ_{C_E}	{0.0132, −0.003 73}	{0.0134, −0.003 66}	{0.986, 1.019}
δ_{C_B}	{0.0547, −0.0308}	{0.0539, −0.0299}	{1.015, 1.035}

The further 100-fold magnification in figure 3 shows the resolution of one of these clusters into the four types of circular polarization singularity described in section 3, identified individually by plotting the four quantities $\mathbf{E}_t \cdot \mathbf{E}_t$, etc, separately. The separations of the singularities are smaller than would be expected on the basis of the rough estimate $\lambda\theta \sim 0.13$, but comparable with $\lambda\theta/2\pi \sim 0.02$. Table 1 shows a comparison of the separations measured from figure 3 with the theoretical formulae (14), (18) and (21), confirming the accuracy of the paraxial theory.

The corresponding linear polarization singularities are shown in figure 4. Note that the ℓ_E and ℓ_B lines are close through most of their length, as predicted by (24), but have different topologies. This reflects the presence of a saddle in the quantity $|E_R|^2 - |E_L|^2$ whose gradient appears in the

denominator of (24), indicating a region where the simple theory fails and the separation of ℓ_E and ℓ_B is larger than $O(1/k^2)$. As expected, the L_E points lie on the ℓ_E lines and the L_B points lie on the ℓ_B lines. Evidently, the positions of these points are determined accurately by the theoretical equations (22), (25) and (26).

To study the approach to paraxiality, we now consider the case where $b_a = b_b = b_c = b$ in (36), so all three polarization ellipses have the same eccentricity. The circular components of the paraxial field (39) then take the simple form

$$\begin{aligned} E_L &= \frac{(1-b)}{\sqrt{2}}\exp(-iky\theta) \\ &\quad\times\left[1-2\cos\left(\frac{\sqrt{3}}{2}kx\theta\right)\exp\left(\frac{3}{2}iky\theta\right)\right] \\ E_R &= \frac{(1+b)}{\sqrt{2}}\exp(-iky\theta) \\ &\quad\times\left[1+2\cos\left(\frac{\sqrt{3}}{2}kx\theta\right)\exp\left(\frac{3}{2}iky\theta\right)\right]. \end{aligned} \tag{40}$$

Apart from a phase, these components are periodic, so the singularities form lattices.

The circular polarization singularities c_E, c_B, C_E and C_B form clusters close to the zeros of E_L and E_R, for which we choose as examples

$$\begin{aligned} &\left\{x=\frac{2\pi}{k\theta 3\sqrt{3}},\ y=0\right\} \quad (E_L=0,\ \text{i.e. right-handed}) \\ &\left\{x=\frac{4\pi}{k\theta 3\sqrt{3}},\ y=0\right\} \quad (E_R=0,\ \text{i.e. left-handed}). \end{aligned} \tag{41}$$

The paraxial displacements of the c_B, C_E and C_B points from the c_E point can now be calculated analytically from the formulae in section 3, leading to

$$\begin{aligned} \boldsymbol{\delta}_{c_B} &= \begin{cases} \dfrac{2\theta(1+b)}{3k(1-b)}\mathbf{e}_x & \text{(right-handed)} \\ \dfrac{2\theta(1-b)}{3k(1+b)}\mathbf{e}_x & \text{(left-handed)} \end{cases} \\ \boldsymbol{\delta}_{C_E} &= \begin{cases} \dfrac{\theta(1+b)}{12k(1-b)}\mathbf{e}_x & \text{(right-handed)} \\ -\dfrac{\theta(1-b)}{12k(1+b)}\mathbf{e}_x & \text{(left-handed)} \end{cases} \\ \boldsymbol{\delta}_{C_B} &= \begin{cases} \boldsymbol{\delta}_{c_B}-\dfrac{\theta(1+b)}{12k(1-b)}\mathbf{e}_x & \text{(right-handed)} \\ \boldsymbol{\delta}_{c_B}+\dfrac{\theta(1-b)}{12k(1+b)}\mathbf{e}_x & \text{(left-handed).} \end{cases} \end{aligned} \tag{42}$$

Several conclusions follow from these results. First, the four singularities in each cluster lie on a straight line (parallel to $\mathbf{e}_x$,); this feature, specific to the case where all b_i are the same, appears in some of the singularities observed experimentally, as can be seen by superposing figures 2 and 4 of [2]. Second, the separations of singularities in left-handed clusters are smaller than those in right-handed clusters by a factor $(1-b)^2/(1+b)^2$, which for $b = 0.8$ is 0.012. This seems to be reflect the non-rigorous distinction made by Hajnal between 'strong' and 'weak' c points: strong c points are those

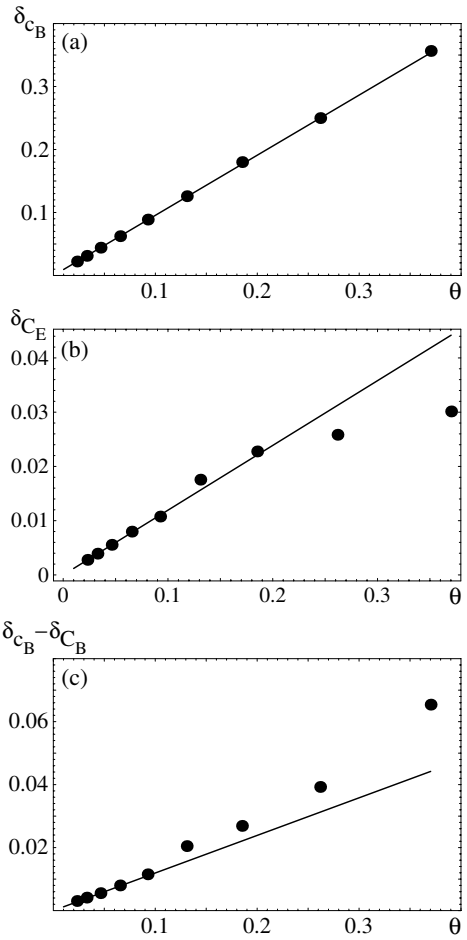

Figure 5. Separations of circular polarization singularities, for $b_a = b_b = b_c = b = 0.8$, calculated from the exact fields (36)–(38) (dots) and from the paraxial theory (42) (full lines), (a) separation of c_B and c_E, (b) separation of C_E and c_E, (c) separation of c_B and C_B. The upper limit of θ is 21°.

with the opposite hand to the three waves comprising the field and are less vulnerable to paraxial perturbation than the weak c points, which have the same hand as the waves in the field; the distinction is not a general one but reflects the fact that all waves in the beam have the same hand. Third, because of the numerical factors in (42), the separations between the two E singularities (c_E and C_E), and between the two B singularities (c_B and C_B), are much smaller (up to 10 times) than the separations between the two c singularities and the two C singularities.

Figure 5 shows the convergence of the separations between the right-handed ('weak') circular polarization singularities to those predicted by the paraxial theory (42) as θ becomes smaller. The range over which the paraxial theory is accurate is much larger for the two c singularities (figure 5(a)) than for the other separations.

Acknowledgments

I thank Dr M R Dennis and Professors J H Hannay and J F Nye for helpful conversations. My research is supported by the Royal Society.

References

[1] Nye J F and Hajnal J V 1987 The wave structure of monochromatic electromagnetic radiation *Proc. R. Soc.* A **409** 21–36

[2] Hajnal J V 1990 Observation of singularities in the electric and magnetic fields of freely propagating microwaves *Proc. R. Soc.* A **430** 413–21

[3] Nye J F 1983 Lines of circular polarization in electromagnetic wave fields *Proc. R. Soc.* A **389** 279–90

[4] Nye J F 1983 Polarization effects in the diffraction of electromagnetic waves: the role of disclinations *Proc. R. Soc.* A **387** 105–32

[5] Hajnal J V 1987 Singularities of the transverse fields of electromagnetic waves. I. Theory *Proc. R. Soc.* A **414** 433–46

[6] Hajnal J V 1987 Singularities in the transverse fields of electromagnetic waves. II. Observations on the electric field *Proc. R. Soc.* A **414** 447–68

[7] Nye J F 1991 Phase gradient and crystal-like geometry in electromagnetic and elastic wavefields *Sir Charles Frank, O.B.E.; an Eightieth Birthday Tribute* ed R G Chambers, J E Enderby, A Keller, A R Lang and J W Steeds (Bristol: Adam-Hilger) pp 220–31

[8] Berry M V and Dennis M R 2001 Polarization singularities in isotropic random waves *Proc. R. Soc.* A **457** 141–55

[9] Berry M V 2001 Geometry of phase and polarization singularities *Singular Optics 2000* vol 4403, ed M Soskin (Alushta, Crimea: SPIE) pp 1–12

[10] Dennis M R 2002 Polarization singularities in paraxial vector fields: morphology and statistics *Opt. Commun.* **213** 201–21

[11] Berry M V 1998 Wave dislocations in nonparaxial Gaussian beams *J. Mod. Opt.* **45** 1845–58

[12] Nye J F 1999 *Natural Focusing and Fine Structure of Light: Caustics and Wave Dislocations* (Bristol: Institute of Physics Publishing)

[13] Berry M V 1984 Quantal phase factors accompanying adiabatic changes *Proc. R. Soc.* A **392** 45–57

[14] Berry M V 1987 The adiabatic phase and Pancharatnam's phase for polarized light *J. Mod. Opt.* **34** 1401–7

[15] Series G W 1975 *The Collected Works of S Pancharatnam* (Oxford: Oxford University Press)